LAWRENCE
LIVERMORE
NATIONAL
LABORATORY

UCRL-JRNL-227803

The groundwater-land-surface-atmosphere connection: soil moisture effects on the atmospheric boundary layer in fully-coupled simulations

R. M. Maxwell, F. K. Chow, S. J. Kollet

February 6, 2007

Advances in Water Resources

Disclaimer

The groundwater-land-surface-atmosphere connection: soil moisture effects on the atmospheric boundary layer in fully-coupled simulations

Reed M. Maxwell, Fotini Katopodes Chow*, and Stefan J. Kollet

Atmospheric, Earth, and Energy Department, Lawrence Livermore National Laboratory, Livermore, California

*Department of Civil and Environmental Engineering, University of California, Berkeley, California

Submitted to Advances in Water Resources.

February 2, 2007

Abstract

This study combines a variably-saturated groundwater flow model and a mesoscale atmospheric model to examine the effects of soil moisture heterogeneity on atmospheric boundary layer processes. This parallel, integrated model can represent spatial variations in land-surface forcing driven by three-dimensional (3D) atmospheric and subsurface components. The development of atmospheric flow is studied in a series of idealized test cases with different initial soil moisture distributions generated by an offline spin-up procedure or interpolated from a coarse-resolution dataset. These test cases are performed with both the fully-coupled model (which includes 3D groundwater flow and surface water routing) and the uncoupled atmospheric model. The effects of the different soil moisture initializations and lateral subsurface and surface water flow are seen in the differences in atmospheric evolution over a 36-hour period. The fully-coupled model maintains a realistic topographically-driven soil moisture distribution, while the uncoupled atmospheric model does not. Furthermore, the coupled model shows spatial and temporal

correlations between surface and lower atmospheric variables and water table depth. These correlations are particularly strong during times when the land surface temperatures trigger shifts in wind behavior, such as during early morning surface heating,

1. Introduction

The characteristics of the land surface determine sensible and latent heat exchange with the atmosphere, thus affecting the evolution of the atmospheric boundary layer. Mesoscale atmospheric models currently rely on parameterized land-surface model (LSM) to provide fluxes of heat, momentum, and moisture from the land surface to the atmosphere. Land-surface models have evolved from so-called leaky-bucket parameterizations (Manabe et al. 1965) to more sophisticated parameterizations (see e.g. the review by Betts et al. 1996). Commonly-used models have been summarized and evaluated in the literature associated with inter-comparison studies (the Project for Intercomparison of Land-Surface Parameterization Schemes, e.g. Henderson-Sellers and Henderson-Sellers 1995; Shao and Henderson-Sellers 1996; Chen et al 1997; Qu et al 1998; Lohmann et al 1998; Pitman et al 1999; Schlosser et al 2000; Luo et al. 2003). While improvements have been made by tuning land-surface model parameters for a variety of test cases, LSMs are all limited to vertical transport in the soil column. They are thus unable to capture topographically-driven lateral variations in soil moisture and limited in their ability to provide spatial variability in predicted land surface fluxes. Current mesoscale atmospheric models are therefore not provided with realistic boundary conditions at the surface because LSMs cannot represent surface and subsurface lateral transport due to topography or moisture gradients. This can lead to errors in model predictions during periods when thermal forcing dominates the diurnal development of the boundary layer (see e.g. Chow et al. 2006a).

The focus of this work is to understand the influence of soil moisture variability on atmospheric boundary layer forcing. This requires the development of a three-dimensional, fully-coupled groundwater-atmospheric flow model, as described in this paper.

Soil moisture and ground surface temperature variability effects on the atmospheric boundary layer have been shown through several previous studies both in idealized and realistic cases. Ookouchi et al. (1984) and Banta and Gannon (1995) showed that changes in soil moisture affect thermally-forced winds on a sloped surface, because the soil wetness determines land surface thermal conductivity and hence surface heat fluxes. Patton et al (2005) used idealized striped wet-dry soil moisture patterns to show that the development of convective cells in the atmospheric boundary layer directly relate to the wet-dry soil patterns. The influence of the land surface on the boundary layer extends further than the development of convection cells, because these then influence the development of clouds and precipitation. Indeed, Chen and Avissar (1994) showed that a soil moisture discontinuity affects wind, cloud and precipitation dynamics in a two-dimensional idealized domain. Clark et al. (2004) used a three-dimensional model to demonstrate that rainfall locations and intensities are affected by the locations and size of a wet soil patch and that these interactions may persist on scales as small as 10-15 km.

Real case studies also indicate the extent of the influence of soil moisture variability on the atmosphere. Taylor et al. (1997) used observational data to study land-atmosphere interactions in semiarid conditions. They provide evidence that boundary layer variability is linked to antecedent rainfall and suggest that soil moisture patterns play a role in rainfall locations. Such observational evidence has led to modeling studies which attempt to improve representation of soil moisture processes. The effect of improved soil moisture data and land-surface parameterizations in simulations of conditions during the Southern Great Plains

experiment in July 1997 was examined by Desai et al. (2005), who showed mixed results on the extent of the influence of soil moisture changes on dry sunny days. Chow et al. (2006a) found that soil moisture initialization was a crucial factor in accurate simulations of thermally-forced valley wind systems in the Swiss Alps using the ARPS (Advanced Regional Prediction System) mesoscale model. An off-line hydrologic model was used to more accurately represent spatial variability of soil moisture in the valley, significantly improving prediction of wind transitions in the valley. Holt et al. (2006) investigated the effects on weather prediction of different initial soil moisture distributions and land surface parameterizations over the IHOP domain. They found that both the different soil moisture initializations and different land parameterizations significantly altered the forecasts.

As LSMs have traditionally ignored the deeper soil moisture processes and the saturated zone (i.e. groundwater), there has been recent interest in incorporating a groundwater component into LSMs to improve the representation of soil moisture at the land surface. Liang et al. (2003) and Yeh and Eltihir (2005) incorporated groundwater processes into a land surface model at larger scales and demonstrated feedbacks on the land surface. Maxwell and Miller (2005) coupled a variably saturated groundwater model to a land surface model and showed the importance of including an explicit representation of the water table on shallow soil moisture distribution.

There has also been work to examine the coupling between the deeper subsurface and the atmosphere. Quinn et al. (1995) coupled the simplified, single-column SLAB boundary layer model to the TOPMODEL land-surface model to investigate the role of groundwater on boundary layer development. They studied wet and dry conditions and identified cases where increased physical complexity of the subsurface is warranted. York et al. (2002) studied the

effects of a single-column atmospheric model connected to a single layer groundwater model through a reservoir-type land surface scheme. They focused on a small watershed in Kansas and found an effect of water levels on surface evapotranspiration. These studies all point to the need for better understanding of physical processes that occur at the interfaces between the deeper subsurface and land surface, and between the land surface and the atmosphere. LSMs are the current numerical mechanism which represents the latter. While LSMs have grown in sophistication, until this current study lateral flow (subsurface and overland) has not been explicitly accounted for.

The full effects of lateral surface and sub-surface flow and, consequently, land-surface properties on the development of the atmospheric boundary layer remain unknown. Open questions remain regarding the effect to which land-surface heterogeneity is reflected in atmospheric heterogeneity, the time and spatial scales over which the effect of soil moisture variations persist in the atmosphere, and how best to represent these processes for numerical simulations of atmospheric flow and transport over a watershed, and eventually over a larger region.

This paper describes the development and application of a dynamically coupled, variably-saturated groundwater, overland-flow, mesoscale atmospheric model (see also Chow et al. 2006b). This model is used to study the effects of soil moisture heterogeneity and water table depth on boundary layer processes. In particular, we have coupled ParFlow, a three-dimensional, parallel, variably saturated groundwater flow model (Ashby and Falgout 1996; Jones and Woodward 2001), with the Advanced Regional Prediction System (ARPS) mesoscale atmospheric model (Xue et al. 2000, 2001, 2003). ParFlow includes an integrated overland flow component (Kollet and Maxwell, 2006), and thus provides ARPS with soil moisture information

that includes the effects of ponding, runoff, and subsurface flow, including an explicitly-resolved water table. In turn, ARPS, through its land-surface model, provides ParFlow with precipitation and evapotranspiration rates, usually not available in groundwater studies. This leads to a fully-coupled model which can represent spatial variations in land-surface processes and feedbacks, driven by physical processes in the atmosphere and the subsurface.

Our test case is the Little Washita watershed in Oklahoma, which has been the subject of numerous studies and provides a unique source of shallow subsurface, surface, and atmospheric data for validation (e.g. Jackson et al. 1999; Vine et al. 2001; Guha et al. 2003). We use this domain to conduct a series of idealized simulations with quiescent initial winds and no lateral forcing to effectively isolate land-surface forcing from other influences on the development of the boundary layer. These simulations are performed with two different soil moisture initializations based on model spin-up and interpolation of regional datasets. While this paper focuses on idealized simulations, the Little Washita test case was chosen for future fully-coupled studies where synoptic forcing and grid nesting will be incorporated.

2. Model components and coupling

We begin with a description of the individual model components for the atmospheric boundary layer, the land surface, and the subsurface and then describe the fully-coupled model.

a. Atmospheric model: ARPS

ARPS was developed at the Center for Analysis and Prediction of Storms at the University of Oklahoma, and is formulated as a parallel, large-eddy simulation (LES) code that solves the three-dimensional, compressible, non-hydrostatic, spatially-filtered Navier-Stokes equations. ARPS was developed for storm-scale atmospheric simulations and has been extensively tested in

idealized and field applications (Xue et al. 2000, 2001, 2003). ARPS uses fourth-order spatial differencing for the advection terms and second-order schemes for other forcing terms. Temporal discretization is performed using a mode-splitting technique to accommodate high-frequency acoustic waves. The large time steps use the leapfrog method; first-order forward-backward explicit time stepping is used for the small time steps, except for terms responsible for vertical acoustic propagation, which are treated semi-implicitly. For this study solid wall lateral boundary conditions and zero-wind initial conditions are used to isolate the effects of the land-surface on boundary layer development. Initial conditions are provided from NOAA North American Regional Reanalysis (NARR) data as described further below. Full physics parameterizations (e.g. radiation and moisture processes) and land-surface schemes are used as would be done for simulations with realistic synoptic forcing.

The standard (uncoupled) land-surface soil-vegetation model used by ARPS solves energy and moisture budget equations in shallow, two-layer soil columns, as described in detail in Xue et al. (2001) and Ren and Xue (2004). The total soil column extends 1 m below the land surface, and is divided into a 1 cm thick surface layer and a 99 cm thick deep soil layer. Energy and moisture budgets are computed using a force-restore model to allow for vertical transport in each column. One soil column is used for each horizontal grid cell but these columns do not communicate and hence do not allow for surface or subsurface lateral transport. A separate canopy layer is used to account for interception of precipitation and transpiration processes. Clapp and Hornberger (1978) pedotransfer functions are used to describe the variation of soil moisture with pressure. Excess precipitation when the soil is fully saturated is ignored and does not contribute to surface runoff.

ARPS uses 13 soil types (including water and ice), and 14 vegetation classes (following the United States Department of Agriculture classifications). Land use, vegetation, and soil type data are obtained from United States Geological Survey (USGS) STATSGO 30 second global data. Elevation data obtained from the USGS are given at 3 arc second intervals and sampled at 1 km resolution. Initial soil temperature is set equal to the air temperature in the first adjacent grid cell at the surface. Initial soil moisture is obtained either from the NARR data set at 32 km resolution or from an offline spinup process explained in Section 4.2.

b. 3D variably saturated groundwater model: ParFlow

ParFlow is a parallel, variably saturated groundwater flow model, and is described in detail by Ashby and Falgout (1996) and Jones and Woodward (2001). In the mode employed here, it solves the Richards equation in three dimensions using a parallel, globalized Newton method. ParFlow has been modified to optionally include the Common Land Model (CLM) (Dai et al. 2003), as described in Maxwell and Miller (2005), as well as an integrated overland flow module (Kollet and Maxwell 2006), which solves the kinematic wave equation. Thus ParFlow has the unique capability to explicitly resolve streamflow without the use of parameterized river routing subroutines. For the groundwater flow solution, ParFlow employs an implicit backward Euler scheme in time, and a cell-centered finite-difference scheme in space. At the cell interfaces, the harmonic averages of the saturated hydraulic conductivities and a one-point upstream weighting of the relative permeabilities are used. For the overland flow component, ParFlow uses an upwind finite-volume scheme in space and an implicit backward Euler scheme in time. ParFlow requires specification of subsurface hydraulic properties, such as the saturated hydraulic conductivity K_{sat}, porosity, φ, and the van Genuchten parameters for the pressure-saturation relationships.

d. Coupling approach: PF. ARPS

The fully-coupled simulations require the simultaneous solution of the 3D groundwater flow equations (provided by ParFlow) and the 3D atmospheric flow equations (provided by ARPS). The original ARPS land surface model constitutes the interface between ParFlow and ARPS to pass surface moisture fluxes between the two models. This approach is shown in Figure 1. The coupling has been performed by integrating ARPS as a subroutine into ParFlow and creating a numerical overlay of the two soil layers of the land surface model in ARPS with the two soil layers at the land surface in ParFlow. The general solution procedure begins with the explicit advancement of ARPS. An operator-splitting approach is employed allowing the ParFlow model to honor the ARPS internal timestep (1 second for this application), or to take larger timesteps, such as 1 h. Using the operator-splitting approach, surface fluxes that are relevant to ParFlow, such as infiltration and evaporation rates are integrated within ARPS over the entire ParFlow timestep (e.g. 1 hour) and used to provide surface fluxes at the new time for implicit time advancement of ParFlow. For the simulations presented here both atmospheric and subsurface timesteps are set to 1 s (and both the large and small ARPS timesteps are set to 1 s). The subsurface moisture field calculated by ParFlow is passed directly to the land-surface model within ARPS and is used by the land surface model in ARPS in the next time step. The land-surface model is advanced for each internal ARPS time step to provide all the surface fluxes, but the soil moisture values are now specified by ParFlow.

3. Model domain and setup

3.1 Little Washita watershed domain and grid

The Little Washita watershed is located in central Oklahoma and has been the focus of several studies (e.g. Jackson et al. 1999; LeVine et al. 2001; Guha et al. 2003), with the result that it is the source of an extensive observational dataset. Figure 2 shows a map of the watershed. The soil and vegetation cover, shown in Figure 3, is predominately grass with shrubs and trees interspersed, underlain by mostly loamy sand, sand, and smaller coverage of sand and silt loam. A resolution of 1 km is used to represent the watershed area using a grid of 45x32 in the horizontal. ARPS uses 50 grid points in the vertical, with 40 m spacing near the ground and stretched above to give an average spacing of 400 m over the 20 km domain height. ParFlow uses 390 grid points in the vertical with 0.5 m resolution for a subsurface depth of 195 m. We focus on the time period from the Southern Great Plains 1999 experiment (SGP99; LeVine et al. 2001; Guha et al 2003) from 7 am CST on July 9, 1999 to 7 pm CST on July 10, 1999.

3.2. Surface-subsurface input data

The land surface constitutes the upper boundary of the groundwater flow model and is obtained from a processed digital elevation model. The maximum depth of the aquifer below the subsurface is approximately 195 m, with a no-flow boundary condition at the bottom of the computational domain. This results in a variable numbers of grid points in the subsurface. The maximum depth value was chosen from borehole information and results from other studies in the region (e.g. Davis 1955) and facilitates modeling of deep groundwater flow. The large depth of the model domain also ensures that the lower boundary condition does not influence the results at the land surface. The hydraulic properties of the deeper subsurface are average values derived from approximately 200 borehole logs collected in the region. The regionally uniform porosity value of $\varphi = 0.4$ [-] corresponds to the arithmetic average of the borehole data. The

average value of K_{sat} was set to be 10 m/day initially, but was adjusted during spin-up to better match the measured hydrographs along the Little Washita River. The adjusted value is $K_s = 5$ m/day, which is about a factor of five larger than the arithmetic mean from the borehole information. This discrepancy can be explained by the quite limited and uncertain information obtained from the borehole logs and the smoothed topography at 1 km resolution, which results in generally smoother water table relief and thus smaller pressure gradients.

The top two 0.5-m thick layers in ParFlow extending to 1 m depth below the ground surface are considered topsoil. The soil information was derived from the soil cover categories used by ARPS (as shown in Figure 3) and matched to the van Genuchten parameters for each corresponding soil type using the data and analysis in Schaap and Leij (1998). Topographic slopes were derived from the digital elevation model after filling sinks (areas of local convergence in the topography) by locally smoothing the topography. In this study, the Manning's coefficient used in the overland flow module is applied uniformly in space, though it can also be distributed to reflect non-uniform surface roughness. The van Genuchten parameters specified in the deeper subsurface correspond to a sandy loam, which we consider representative for the watershed.

4. Test Cases

4.1. Configuration of test cases

Idealized simulations of the Little Washita watershed are used to study the sensitivity of the evolution of the atmospheric boundary layer to spatial variations in soil moisture and water table depth. While the actual watershed topography and soil and vegetation types are incorporated, we initialize the simulations with zero winds and use solid wall lateral boundary

conditions to isolate the effects of the land surface forcing. Initial potential temperature and humidity are specified with sounding observation data from nearby Norman, OK at 7 am on July 9, 1999. Boundary layer development is driven by the diurnal variations in incoming solar radiation and the consequent land surface fluxes. Three different idealized cases with different soil moisture initializations are performed.

1. First, the stand-alone ARPS model is used with soil moisture interpolated from the NARR dataset; Case 1- referred to as ARPS(narr) for ARPS using NARR soil moisture initialization.
2. Second, the fully-coupled PF.ARPS model is run with the initial soil moisture derived from the offline spin-up procedure described below; Case 2- referred to as PF.ARPS.
3. Finally, to distinguish between the effects of soil moisture initialization and soil moisture evolution, the stand-alone ARPS model is run using the same initial soil moisture provided in Case 2 but without any dynamic coupling to ParFlow; Case 3- referred to as ARPS(os), for ARPS-*O*ffline *S*oil moisture initialization.

Note that Cases 2 and 3 have identical initial soil moisture, Cases 1 and 3 are identical models, and that all cases have identical initial soil temperature distributions. The offline spinup used in Case 2 and 3 is explained in more detail in the following section.

4.2. Offline spin-up

An offline, model spin-up is used to generate realistic initial soil moisture distributions for use in test cases 2 and 3 described above. Spin-up is defined as the dynamic equilibrium of the mass and energy balance over a certain time period over which a time series of atmospheric data is used to repeatedly force the model. To generate the offline spin-up data for initialization,

ParFlow is run coupled with the more advanced land surface model CLM (Dai et al, 2003) driven by atmospheric forcing provided by the NARR reanalysis dataset. The forcing data are for the 1998-1999 water year and include wind speed and direction, surface air temperature, incoming radiation, precipitation, pressure and humidity. This configuration is used for spin-up (rather than using ParFlow with the ARPS land surface model) to more accurately represent thermal, snow and biogeophysical processes in a more sophisticated way (Noilhan and Planton, 1989; Dai et al, 2003). Though no comprehensive calibration process is used, good comparisons with observed time series of streamflow, soil moisture and land energy balance were obtained after repeated application of this meteorological forcing from September 1998 to October 1999 (not shown, Kollet and Maxwell, 2007). As mentioned above, both the Case 2, the fully-coupled PF.ARPS, and Case 3, the uncoupled ARPS(os) simulations, are initialized by the soil moisture fields from July 9, 1999 provided by this spin-up processes. This offline model used for spin-up incorporates more and better process descriptions in contrast to other methods that might calibrate, or tune, land surface parameters, or assimilate land surface data.

4.3. Test case comparisons

Figure 4 shows the soil moisture fields from PF.ARPS, ARPS(os) and ARPS(narr) at 12 hour intervals over the simulation period. The PF.ARPS and ARPS(os) soil moisture fields show the distinct signature of the Little Washita River, with wetter conditions along the river corridor and drier conditions in the uplands. This is due to the convergence of deeper groundwater water flow at discharge zones that are the Little Washita River valley and its tributaries during the offline spin-up processes. Additional variability is a result of the influence of the distributed soil and vegetation cover (as shown in Figure 3), which is, however, less pronounced than the impact

of groundwater dynamics. In contrast, the soil moisture field from the uncoupled ARPS(narr) run shows small spatial variability, due to the use of interpolated coarse-resolution soil moisture data from NARR. Because of the land-surface parameterization in ARPS, the soil moisture values at a given grid cell can only be affected by shallow soil properties at that x, y location, the land cover, soil type, and the atmospheric conditions. Thus the patterns of variability in soil moisture in the ARPS(narr) simulation track closely the variations in soil type and to a lesser extent the variation in vegetation type, as seen by comparing Figure 3 and the last column in Figure 4. The ARPS land surface model is not able to account for topographically-induced lateral groundwater flow and, thus, cannot develop spatial patterns like those from PF.ARPS; the soil moisture field in ARPS(narr) tends to dry out uniformly over the simulation period until isolated precipitation events develop after about 24 hours of simulation (discussed further below).

Even though the PF.ARPS and ARPS(os) models are initialized with the same soil moisture distribution (shown at time zero, in the top panels of Figure 4), the soil moisture in these models begins to show differences as early as 12 hours of simulation time (second panel). These differences are most notable in the upper river valley (west and center part of the domain), in the headwaters (x = 0-15 km, y = 15-25 km), and along the hilltops. This is due, as pointed out above, to the inability of the soil model in ARPS to account for groundwater storage, lateral flow and surface water routing. Over the first 12 hours of simulation time the PF.ARPS model maintains the wet conditions in the river valley by a combination of groundwater storage below the root zone (non-existent in ARPS) and lateral redistribution of water due to topographically driven subsurface flow. These effects are more pronounced later in the simulation (12 h and 24 h, bottom two panels in Figure 4) after rainfall occurs. With no processes to maintain topographic surface and subsurface flow, the rainfall (see Figure 8 later) begins to significantly change the

initial soil moisture distribution, particularly in the ARPS(os), but also the ARPS(narr) case, unlike the PF.ARPS case, which routes rainfall over the surface and in the subsurface. This is seen by the distinct circular patterns of soil moisture for the ARPS(narr) and ARPS(os) simulations in the bottom panel of Figure 4, directly due to the areas of convective rainfall (shown in Figure 8, below).

Figures 5, 6 and 7 plot the soil temperature, latent heat flux and potential temperature (respectively) for the three models for a time series covering early morning on the second simulation day, t = 24, 26 and 27 h (7 am, 9 am and 10 am local time). This time series was chosen because it corresponds to early morning land heating which drives convection. Soil moisture has been shown to play an important role in thermally-forced flows (see e.g. Patton et al. 2005, Chow et al. 2006a). Figure 5 shows that the soil temperature for PF.ARPS and ARPS(os) is quite different than that of the ARPS(narr) case. The soil temperatures exhibit patterns similar to the soil moisture, showing temperature variations between the river valleys and hill tops. For t = 26 and 27 h, cooler temperatures are predicted in the wetter river valleys and warmer temperatures on the drier hill tops. At time t = 24 h, the opposite is true, with warmer temperatures in the river valleys and colder temperatures on the hill tops. The temperature plots show more influence of soil and vegetation cover than the soil moisture profiles. The ARPS(narr) case, again, only shows variation in temperature due to variations in soil and vegetation cover with some slight variations in incoming radiation due to local surface slope changes.

The soil temperatures for PF.ARPS and ARPS(os) in Figure 5 show some minor differences, despite the more significant differences in surface soil moisture shown in Figure 4. The soil temperature determined by the ARPS land surface model comes directly from the

formulation of Noilhan and Planton (1989). In this formulation the surface soil temperature depends on soil moisture from the second, or deeper, soil layer (Noilhan and Planton, 1989; see their Eq. 10), not the upper soil moisture used in other formulations (see e.g. Dai et al, 2003). Soil and vegetation cover are also a factor (see Eq. 8 and Table 2 in Noilhan and Planton, 1989) but as these parameters are the same in all simulations and the deeper soil layer responds more slowly than the upper soil layer, the soil temperatures between PF.ARPS and ARPS(os) are quite similar. The limitations of this aspect of the Noilhan and Planton (1989) approach have been previously discussed by Pleim and Xiu (1995; see their Section 2a) and requires further investigation.

Figure 6 plots the latent heat flux for the three model runs, showing patterns of both soil and vegetation type and soil moisture. While most of the domain is grasslands over loamy sand, a line of open shrub and croplands over loam along the river valley, and an area of crop and shrublands over silt loam in the headwaters area of the watershed are particularly visible. Even though vegetation and soil cover play a large role, soil moisture is a significant moderator of latent heat as demonstrated by the different results from the three simulations. The latent heat flux for the ARPS(narr) simulation is significantly different than for PF.ARPS and ARPS(os). The PF.ARPS and ARPS(os) simulations also show local differences in energy fluxes up to 25%. These differences correspond to both the aforementioned areas of different vegetation cover and soil moisture differences seen in Figure 4. The bare ground evaporation and vegetation transpiration formulations used to determine the latent heat flux in ARPS are described by Noilhan and Planton (1989) and Noilhan and Mahfouf (1996). Soil moisture moderates both processes. Both relationships assume that soil moisture values greater than field capacity (taken as a fraction of saturation which is a function of soil type) present no resistance to evaporation

and transpiration, making the latent heat flux less sensitive in wetter regions. Below field capacity, bare soil evaporation depends upon a sinusoidal relationship to soil moisture, whereas plant transpiration depends linearly on soil moisture. Bare soil evaporation has been shown to be sensitive to the formulation used (e.g. Kondo et al. 1990; Mahfouf and Noilhan, 1991). The role of subsurface water in evapotranspiration will be discussed further below.

Figure 7 plots the potential temperature at the first grid point above the ground for the three simulations. Again, the largest differences are between the ARPS(narr) case and the two cases initialized with the soil moisture fields from the offline spin-up. While the ARPS(narr) case starts with a topographically-influenced potential temperature, this evolves to reflect only the variation in the soil and vegetation cover. The potential temperature for the ARPS(narr) simulation is generally higher than the ARPS(os) and PF.ARPS cases. The PF.ARPS and ARPS(os) cases are similar overall, but the PF.ARPS case shows cooler potential temperatures in a number of locations, reflecting the influence of variations in soil moisture distribution. These changes in the near-surface air temperature demonstrate the direct forcing of the land surface on the atmosphere and will drive different convective processes, as described below.

Figure 8 shows the hourly rainfall distribution for the three cases, PF.ARPS (left), ARPS(os) (center) and ARPS(narr) (right) for two times (33 and 34h) late in the simulation. With no lateral forcing, the rainfall is generated convectively in all three cases and its location and intensity show little agreement between the three cases. The differences in potential temperature shown in Figure 7 trigger convective motions that develop into variable rainfall patterns, demonstrating the sensitivity of the atmosphere to land-surface forcing under calm conditions. The rainfall patterns are particularly strongly reflected in the soil moisture distribution for ARPS(os) and ARPS(narr) at 36 hr as shown previously in the last row of Figure

4. The influence of soil moisture on rainfall was recently studied by Clark et al. (2004), who correlated increased surface soil moisture resulting from antecedent rainfall to specific patterns of rainfall from subsequent frontal storms. While the current study involves a more complicated system than the idealized study of Clark et al. (2004), there may be some similarities between the observed precipitation processes. Figure 8 suggests that rainfall patterns for the PF.ARPS case, with precipitation occurring along the margins of the wet river valleys, might well be influenced by preceding soil moisture patterns. Additional work is needed to examine the mechanisms of these land-atmosphere feedbacks on rainfall, which is beyond the scope of this study.

Summarizing the evolution of soil moisture for the different cases, Figure 9 plots time series of the spatially-averaged surface soil moisture for the three model simulations. PF.ARPS and ARPS(os) start with the same spatial soil moisture distribution, while the ARPS(narr) model is initialized with the drier upper soil layer from NARR data. The ARPS(os) upper soil moisture dries out quite rapidly and is almost in agreement with the ARPS(narr) simulation by 36 hours. The PF.ARPS soil moisture also dries out slightly over the simulation period, but maintains a much wetter upper soil moisture than the ARPS(os) simulation. This further underscores the additional processes present in the fully-coupled PF.ARPS model and how lateral flow and groundwater storage help to maintain a much wetter soil profile.

4.4. PF.ARPS correlations and analysis

The fully-coupled PF.ARPS simulations provide a unique opportunity to evaluate effects of deep subsurface processes on atmospheric boundary layer development. Because the land surface formulation in ARPS includes separate dependence on each shallow soil layers (surface and deep), land heat fluxes depend more strongly on the water table depth than on either the

upper or lower soil moisture alone. As mentioned previously, land surface temperature, for example, depends only on the deeper soil moisture (a limitation noted by Pleim and Xiu, 1995) while bare soil evaporation is a function of upper soil moisture. In the coupled model, PF.ARPS, the soil moisture is modeled as a coherent system from land surface to bedrock, directly accounting for water table storage and lateral flow. This allows correlations between water table and land surface functions to be fully realized in the coupled model.

To investigate the effect of the groundwater component on land surface and atmospheric processes, scatter plots are generated between water table depth (as distance below the land surface) and various surface and subsurface variables. These are either taken at a point in time or averaged over the entire PF.ARPS simulation. Figure 10 plots four such comparisons, for a) surface soil temperature, b) potential temperature, c) boundary layer depth, and d) the vertical wind speed at the surface as a function of water table depth for simulation times 24 h (top), 26 h (middle) and 27 h (bottom) for all surface points in the domain. These plots represent the influence of water table depth on land-surface and atmospheric processes.

At 24 h, there is a negative correlation in surface soil temperature to water table depth with two patterns present, one for water table depths less than one meter and the other for water table depths greater than one meter. The ground surface temperatures corresponding to water table depths of less than one meter are in general warmer than the ground surface temperatures corresponding to water table depths greater than one meter, though there is significant scatter in the relationship. There is a weak trend in increasing surface air (potential) temperature with increasing water table depth, though with significant scatter. There is also a weak correlation between boundary layer depth and water table depth, and we see a weak negative correlation between the vertical wind component at the bottom atmospheric cell, w, and water table depth.

As the land surface temperature increases during sunrise (times 26 and 27h), we see a reversal in correlation between upper soil temperature and water table depth, with soil temperature increasing with increasing water table depth. The potential temperature correlation with water table depth strengthens over these times as well, with less scatter apparent at 27 hours than at 24 hours of simulation time. The entire boundary layer becomes deeper and exhibits a stronger correlation to water table depth. The vertical velocity component also changes its correlation to water table depth, shifting to a positive correlation at 27 hours of simulation time to increasing water table depth, with mostly downward velocities at very shallow and upward velocities at deeper water table depth values. This corresponds to the onset of convection with downward velocities in the cooler river valleys and upward velocities at the warmer hill tops. The timing of this shift in convective behavior can be important in some systems, particularly thermally-forced slope flows. Modeling such wind transitions has been shown to be sensitive to soil moisture distribution (see e.g. Chow et al 2006a, Daniels et al 2006).

Figure 11 shows latent heat flux, averaged in time over the simulation, as a function of water table depth for a range of soil types and vegetation cover. Time averages over the duration of the simulation indicate the influence of water table depth with the shorter-term variability in other processes removed (e.g. solar forcing), thus showing which land-surface and atmospheric parameters might be correlated with water table depth over longer timescales. We see a relationship between latent heat flux and water table depth for some soil and vegetation types. The correlations between water table depth and latent heat flux are strongest for loamy sand (top middle panel). There are greater latent heat fluxes from areas in the domain with shallower water table depths and lower latent heat fluxes from areas with deeper water table depths. This corresponds to lower latent heat fluxes from the drier hill tops and greater latent heat fluxes from

the wetter river valleys. We also see a negative correlation of latent heat flux with water table depth for open shrublands over loam, for trees over silt loam, and for sand, though there are only two locations in the domain where sand corresponds to a water table depth of less than one meter. For silt loam covered by grass or by open shrublands there is a weak correlation of latent heat flux with water table depth. This is also true for loam covered by grasslands. These relationships reflect the fact that many parameters that influence heat flux (soil moisture retention parameters, saturated hydraulic conductivity, and vegetation parameters) are all a function of soil type and vegetation cover. Figure 11 illustrates that while correlations are present between latent heat flux and water table depth, they also vary with soil type and land cover. The variations that water table depth imparts on latent heat flux, are as large as those imparted by variations in soil type and land cover. This is demonstrated by the range of heat flux variation with water table depth, on the order of 100 W/m^2 for loamy sand, being as great as or greater than the difference in heat fluxes observed between grasslands and trees. This provides strong motivation to include not only soil vegetation type but also water table influences in land-surface models for use with mesoscale atmospheric models.

Figures 12a shows the potential temperature, averaged in time over the simulation, as a function of water table depth, demonstrating a positive correlation between potential temperature and water table depth over all soil and land cover types, similar to that seen for times t = 24, 26, and 27 h in Figure 10. Figure 12b shows potential temperature as a function of water table depth for loamy sand (all vegetation types) and loam covered by open shrublands, the two categories with the strongest correlation between latent heat flux and water table depth shown in Figure 11. We see that these two soil and land cover types account for some of the scatter in Figure 12a. This figure suggests that potential temperature is not only correlated to water table depth at

instances in time (e.g. Figure 10) but that longer-term correlations may persist. Additionally, though there appears to be an influence of soil and land cover type on potential temperature, this influence is smaller than the influence of water table depth, again pointing to the need to include the effect of water table depth in land-surface models.

5. Summary and Conclusions

This paper presents the methodology for a fully-coupled, parallel, groundwater, overland flow, land-surface, and atmospheric model. Our fully-coupled model incorporates three-dimensional subsurface flow and surface water routing into a mesoscale atmospheric flow model to better represent spatial variations in soil moisture. Results from the coupled model are compared to those from an uncoupled atmospheric model using a realistic test case with idealized boundary conditions. These results indicate the potential to improve predictions of boundary layer processes by incorporating physical processes at the land surface and below. We have demonstrated the sensitivity of thermally-forced boundary layer development to surface moisture and temperature conditions and our ability to more realistically represent the spatial variability in surface forcing using our coupled modeling approach.

A realistic initial spatial distribution of soil moisture can be generated using an offline spinup procedure to incorporate subsurface and surface processes forced by atmospheric data over a water year. The results can be used to provide improved initial conditions to mesoscale meteorological models. Other researchers (e.g. Holt et al, 2006) have shown this in an assimilation framework, it is shown here with improved surface-subsurface processes.

The initial distribution of soil moisture has a strong effect on the development of the atmospheric boundary layer under calm conditions. If lateral flow is not accounted for, this soil

moisture distribution can decay during a 36-hour period, a time period shorter than many weather forecast periods. Lateral surface and subsurface flow is important to maintain topographically-induced drainage and soil moisture patterns over short (hour) timescales, as shown by comparisons between PF.ARPS and ARPS(os) runs in Figures 4-9 and can affect potential temperature and wind direction and speed over these timescales.

The interplay between soil and land cover and surface and subsurface moisture transport is quite complex and appears to be highly dependent on the particular formulations used in the land surface parameterization and deserve further examination and validation.

Correlations exist between water table depth and ground surface temperature, potential temperature in the first atmospheric cell above the land surface, and transient boundary layer development. Correlations are particularly strong during warm/cold transitions when surface heating determines boundary layer growth.

The coupled model shows correlation between water table depth and latent heat flux and potential temperature averaged over the simulation time of 36h. This suggests that these correlations may also persist over longer timescales.

The correlations between water table depth and land surface and atmospheric processes shown in Figure 11 explain much of the sensitivities that other researchers have seen (e.g. Chow et al 2006a; Holt et al 2006). The absence of these correlations under varying conditions (at different times or depending upon land and soil cover) also explains cases in which other studies have seen less sensitivity of boundary layer processes to land surface conditions (e.g. Desai et al 2005). The correlations shown in this work between water table and surface and boundary layer processes are testable in the field using collocated measurements of subsurface and atmospheric properties and parameters, which are currently lacking. This work and follow-up work of this

kind should guide field experiments and campaigns to understand whether these correlations are seen in nature which will lead to further understanding of interactions of the subsurface and the atmosphere.

The largest differences in the idealized sensitivity simulations were between the ARPS(narr) stand-alone and the PF.ARPS simulations, clearly showing the inadequacy of typical land surface models in representing spatial variability at the land surface due to topographic variations. The PF.ARPS and ARPS(os) results did not deviate greatly, but still showed different rainfall patterns. The ARPS(os) results indicate that ARPS could be used in stand-alone mode if initialized with offline spin-up data to provide realistic spatially distributed soil moisture; ARPS could then be run over a short simulation period such as 24 hours, allowing a more practical application scenario for forecast-like simulations where lateral subsurface transport may not be as important as the soil moisture initialization. For longer-term simulations, the fully 3D coupled subsurface and atmospheric model is needed to fully incorporate the feedbacks between the atmospheric boundary layer and the subsurface. Examples of simulations requiring full coupling include seasonal simulations for regional climate prediction. Fully-coupled runs may also be useful for flood forecasting and in other cases where surface water routing and immediate feedbacks to the atmosphere are critical (see e.g. Sturdevant-Rees et al 2001, Castillo et al. 2003).

The additional computational costs for PF.ARPS are 3-50% greater than for ARPS alone (depending upon the size of the subsurface and the timestep operator splitting); given the potential improvements of the improved land-surface feedback, this cost is warranted. Furthermore, as our approach is fully parallel, the additional computational costs may be offset through the use of larger parallel systems.

Our coupled modeling approach is general, allowing for physically-accurate representation of subsurface, land-surface, and atmospheric processes; no previous atmospheric-land-surface model combination is able to capture all of these processes. Because the fully-coupled model, PF.ARPS, is initialized using an offline spin-up process with atmospheric forcing data, calibration or tuning requirements are minimized. This demonstration study was performed with idealized boundary conditions to isolate the effects of the land surface on the atmosphere. Future work will apply PF.ARPS to larger domains with synoptic lateral forcing where the effects of soil moisture on model comparisons to observation data may be studied. Higher-resolution simulations will also be pursued to investigate the effect of topography representation for surface water routing in the watershed. Additionally, PF.ARPS can be used to study the effect of land-surface processes on regional climate predictions on seasonal time scales. Incorporation of lateral moisture transport through subsurface flow may be of even greater importance on these larger space and time scales.

6. Acknowledgements

This work was conducted under the auspices of the U. S. Department of Energy by the University of California, Lawrence Livermore National Laboratory (LLNL) under contract W-7405-Eng-48 and was supported by the LLNL Laboratory Directed Research and Development Program at LLNL. We are grateful for the efforts of Q. Duan and P. Granvold in support of this project.

7. References

Ashby, S. F. and R. D. Falgout, 1996: A parallel multigrid preconditioned conjugate gradient algorithm for groundwater flow simulations. Nuclear Science and Engineering, 124, 145–159.

Avissar, R. and R. Pielke, 1989: A parameterization of heterogeneous land-surface for atmospheric numerical models and its impact on regional meteorology. Monthly Weather Revview, 117, 2113-2136

Banta, R. M. and P. T. Gannon, 1995: Influence of soil moisture on simulations of katabatic flow. *Theor. Appl. Climatol.*, **52**, 85 – 94.

Betts, A., J. Ball, A. Belijaar, M. Miller, and P. Viterbo, 1996: The land surface-atmosphere interaction: A review based on observational and global modeling perspectives. Journal of Geophysical Research, 101, 7209–7225.

Castillo, V.M., Gomez-Plaza, A., and M. Martinez-Mena, 2003: The role of antecedent soil water content in the runoff response of semiarid catchments: a simulation approach. Journal of Hydrology, 284 (1-4), 114-130.

Chen, F. and R. Avissar, 1994: Impact of Land-Surface Moisture Variability on Local Shallow Convective Cumulus and Precipitation in Large-Scale Models, Journal of Applied Metereology, 33, 1382-1401.

Chen, T. and Coauthors, 1997: Cabauw experimental results from the project for intercomparison of land-surface parameterization schemes. Journal of Climate, 10, 1194–1215.

Chow, F. K., A. P. Weigel, R. L. Street, M. W. Rotach, and M. Xue, 2006a: High-resolution large-eddy simulations of flow in a steep Alpine valley. Part I: Methodology, verification, and sensitivity studies. Journal of Applied Meteorology and Climatology , 45, 63–86.

Chow, F.K., Kollet, S.J., Maxwell, R.M., and Q. Duan. 2006b. Effects of soil moisture heterogeneity on boundary layer flow with coupled groundwater, land-surface, and mesoscale atmospheric modeling. Paper 5.6. 17th Symposium on Boundary Layers and Turbulence, American Meteorological Society, 6 pages.

Clapp, R.B. and G.M. Hornberger, 1978: Empirical equations for some hydraulic properties. Water Resources Research, 14, 601-604.

Clark, D.B., C.M. Taylor and A.J. Thorpe, 2004: Feedback between the Land Surface and Rainfall at Convective Length Scales. Journal of Hydrometeorology, 5, 625-639.

Dai, Y., X. Zeng, R. Dickinson, I. Baker, G. Bonan, M. Bosilovich, A. Denning, P. Dirmeyer, P. Houser, G. Niu, K. Oleson, C. Schlosser, and Z. Yang, 2003: The common land model. Bulletin of the American Meteorological Society , 84, 1013– 1023.

Davis, L. V., 1955: Geology and ground water resources of frady and nothern stephens counties, Oklahoma. Bulletin no. 73, Oklahoma Geological Survey.

Desai, A. R., K. J. Davis, C. J. Senff, S. Imail, E. Browell, D. R. Stauffer, and B. P. Reen, 2005: A case study on the effects of heterogeneous soil moisture on mesoscale boundary-layer structure in the Southern Great Plains, U.S.A. Part I: simple prognostic model. Boundary-Layer Meteorology , 119, doi:10.1007/s10546–005–9024–6.

Guha, A., J. M. Jacobs, T. J. Jackson, M. H. Cosh, E.-C. Hsu, and J. Judge, 2003: Soil moisture mapping using ESTAR under dry conditions from the Southern Great Plains experiment (SGP99). IEEE Transactions on Geoscience And Remote Sensing, 41, 2392–2397.

Henderson-Sellers, A. and B. Henderson-Sellers, 1995: Simulating the diurnal temperature range: Results from phase 1(a) of the project for intercomparison of landsurface parameterisation schemes (PILPS). Atmospheric Research, 37, 229–248.

Holt, T.R., D. Niyogi, F. Chen, K. Manning, M. LaMone and A. Qureshi, 2006. Effect of land–atmosphere interactions on the IHOP 24–25 May 2002 convection case. Monthly Weather Review, 134, 113-123.

Jackson, T. J., D. M. L. Vine, A. Y. Hsu, A. Oldak, P. Starks, C. T. Swift, J. D. Isham, and M. Haken, 1999: Soil moisture mapping at regional scales using microwave radiometry: The Southern Great Plains Hydrology Experiment. IEEE Transactions on Geoscience And Remote Sensing, 37, 2136–2151.

Jones, J. E. and C. S. Woodward, 2001: Integrated surface-groundwater flow modeling: a free-surface overland flow boundary condition in a parallel groundwater flow model. Advances in Water Resources, 24, 763–774.

Kollet, S.J. and R.M. Maxwell, 2007: Investigating the influence of water table dynamics on land surface processes using a fully-coupled, distributed watershed model. *In preparation*, to be submitted to Water Resources Research.

Kollet, S. J. and R. M. Maxwell, 2006: Integrated surface-groundwater flow modeling: a free-surface overland flow boundary condition in a parallel groundwater flow model. Advances in Water Resources, 29, 945-958.

Kondo, J., N. Saigusa and T. Sato, 1990: A parameterization of evaporation from bare soil surfaces, Journal of Applied Meteorology, 29, 385-389.

Liang, X., Z. Xie, and M. Huang, 2003: A new parameterization for surface and groundwater interactions and its impact on water budgets with the variable infiltration capacity (VIC) land surface model. Journal of Geophysical Research, 198, 1194–1215.

Lohmann, D. and Coathors, 1998: The project for intercomparison of land-surface parameterization schemes PILPS phase 2(c) Red Arkansas River basin experiment: 3. spatial and temporal analysis of water fluxes. Global and Planetary Change, 19, 161–179.

Luo, L., , and Coauthors, 2003: Effects of frozen soil on soil temperature, spring infiltration, and runoff: Results from the PILPS 2(d) experiment at Valdai, Russia. Journal of Hydrometeorology , 4, 334–351.

Mahfouf, J.F. and J. Noilhan, 1991: Comparative study of various formulations of evaporation from bare soil using in situ data. Journal of Applied Meteorology, 30, 1354-1365.

Manabe, S., J. Smagorinksy, and R. Strickler, 1965: Simulated climatology of a general circulation model with a hydrologic cycle. Monthly Weather Review , 93, 769–798.

Maxwell, R. and N. Miller, 2005: Development of a coupled land surface and groundwater model. Journal of Hydrometeorology, 6, 233–247.

Noilhan, J. and S. Planton, 1989: A simple parameterization of land surface processes for meteorological models. Monthly Weather Review, 117, 536-549.

Noilhan, J. and J.-F. Mahfouf, 1996: The ISBA land surface parameterization scheme. Global and Planetary Change, 13, 145-159.

Ookouchi, Y., M. Segal, R. C. Kessler, and R. A. Pielke, 1984: Evaluation of soil moisture effects on the generation and modification of mesoscale circulations. *Mon. Wea. Rev.*, **112**, 2281 – 92.

Patton, E.G., P.P. Sullivan and C-H Moeng, 2005. The influence of idealized heterogeneity on wet and dry planetary boundary layers coupled to the land surface, Journal of the Atmospheric Sciences, 62, 2078-2097.

Pitman, A. and Coauthors, 1999: Key results and implications from phase 1(c) of the project for intercomparison of land-surface parameterization schemes. Climate Dynamics, 15, 673–684.

Pleim, J.E. and A. Xiu, 1995: Development and testing of a surface flux and planetary boundary layer model for application in mesoscale models. Journal of Applied Meteorology, 34, 16-32.

Qu, W. and Coauthors, 1998: Sensitivity of latent heat flux from PILPS land-surface schemes to perturbations of surface air temperature. Journal of Atmospheric Sciences, 55, 1909–1927.

Ren, D. and M. Xue, 2004: A revised force-restore model for land surface modeling. Journal of Applied Meteorology, 43, 1768– 1782.

Schaap, M. G. and F. J. Leij, 1998: Database-related accuracy and uncertainty of pedotransfer functions. Soil Science, 163, 765–779.

Schlosser, C. and Coathors, 2000: Simulations of a boreal grassland hydrology at Valdai, Russia: PILPS phase 2(d). Monthly Weather Review , 128, 301–321.

Shao, Y. and A. Henderson-Sellers, 1996: Modeling soil moisture: A project for intercomparison of land surface parameterization schemes phase 2(b). Journal of Geophysical Research, 101, 7227–7250.

Sturdevant-Rees, P., Smith, J.A., Morrison J., and M. L. Baeck, 2001: Tropical storms and the flood hydrology of the central Appalachians. Water Resources Research, 37 (8), 2143-2168.

Taylor, C.M., F. Said and T. Lebel, 1997: Interactions between the Land Surface and Mesoscale Rainfall Variability during HAPEX-Sahel. Monthly Weather Review, 125, 2211-2227.

Vine, D. M. L., T. J. Jackson, C. T. Swift, M. Haken, and S. W. Bidwell, 2001: ESTAR Measurements during the Southern Great Plains experiment (SGP99). IEEE Transactions on Geoscience And Remote Sensing, 39, 1680–1685.

Xue, M., K. K. Droegemeier, and V. Wong, 2000: The advanced regional prediction system (ARPS): A multi-scale non-hydrostatic atmospheric simulation and prediction model. Part I: Model dynamics and verification. Meteorology and Atmospheric Physics, 75, 161–193.

Xue, M., K. K. Droegemeier, V. Wong, A. Shapiro, K. Brewster, F. Carr, D. Weber, Y. Liu, and D. Wang, 2001: The advanced regional prediction system (ARPS): A multi-scale non-hydrostatic atmospheric simulation and prediction tool. Part II: Model physics and applications. Meteorology And Atmospheric Physics, 76, 143–165.

Yeh, P.-F. and E. Eltahir, 2005: Representation of water table dynamics in a land-surface scheme. Part I: Model development. Journal of Climate, 18, 1861–1880.

York, J. P., M. Person, W. J. Gutowski, and T. C. Winter, 2002: Putting aquifers into atmospheric simulation models: an example from the Mill Creek watershed, northeastern Kansas. Advances in Water Resources, 25, 221–238.

8. Figures

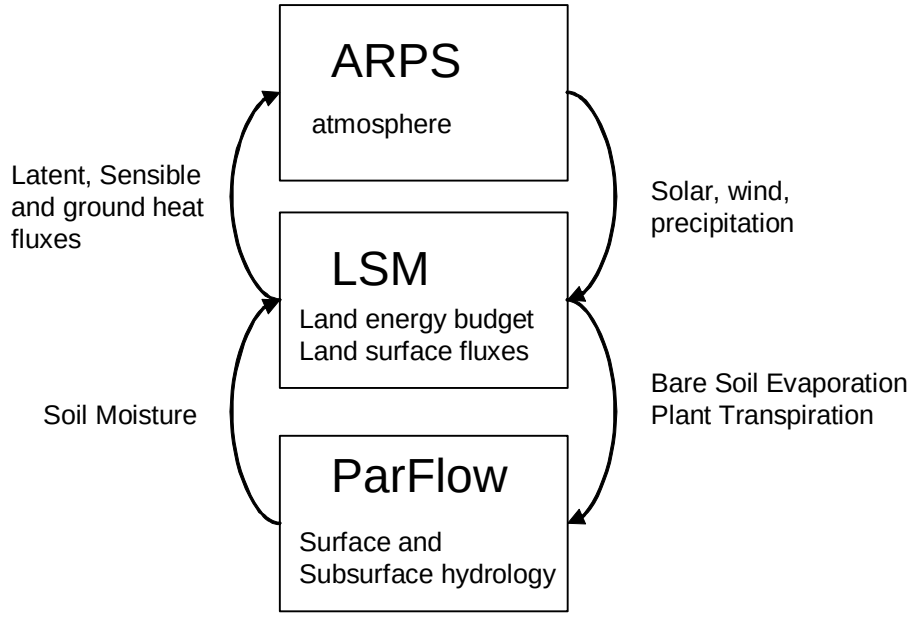

Figure 1. Simplified flowchart of coupled model process.

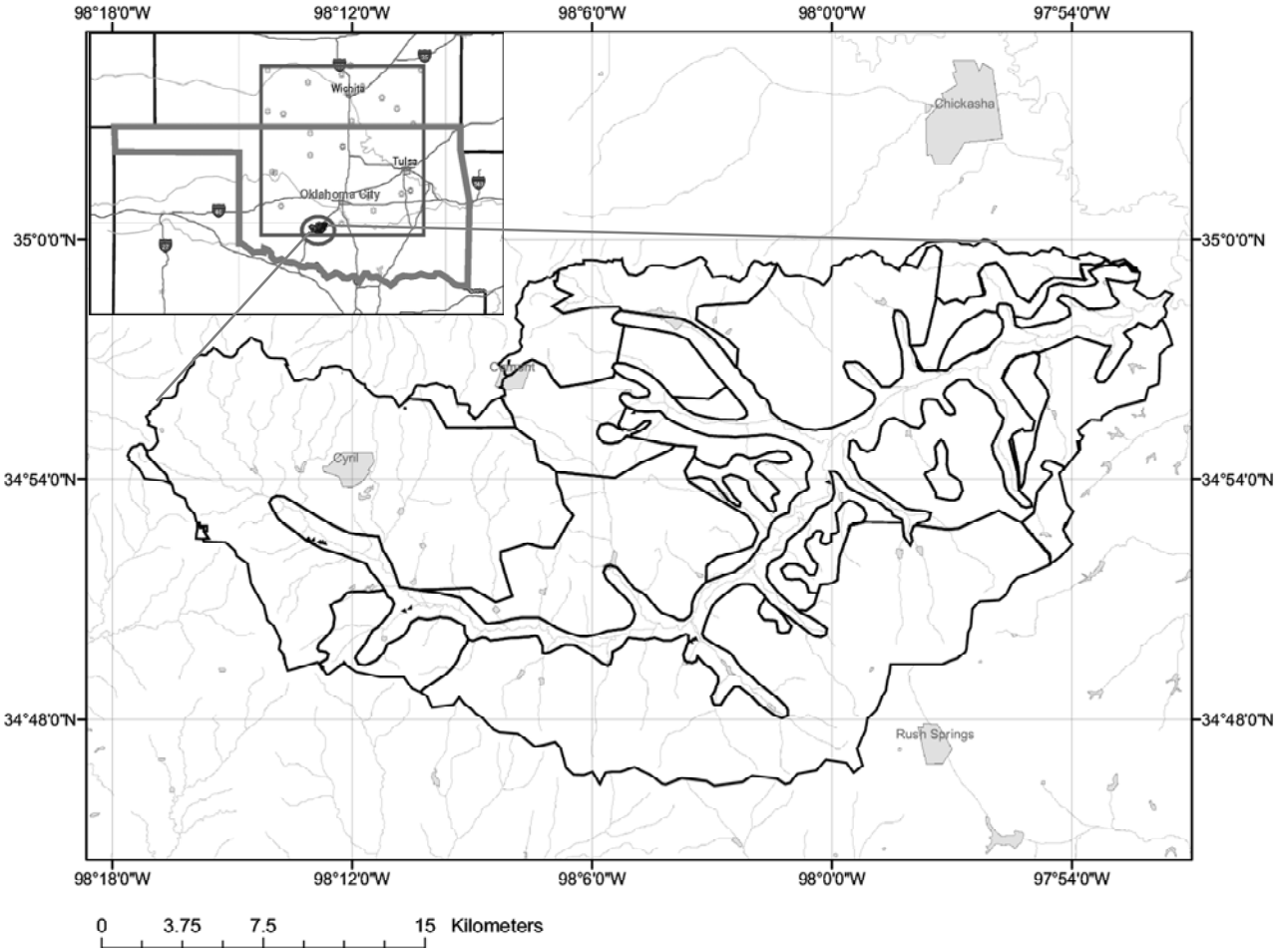

Figure 2. Location of the Little Washita watershed. The inset shows the location of the watershed in the state of Oklahoma.

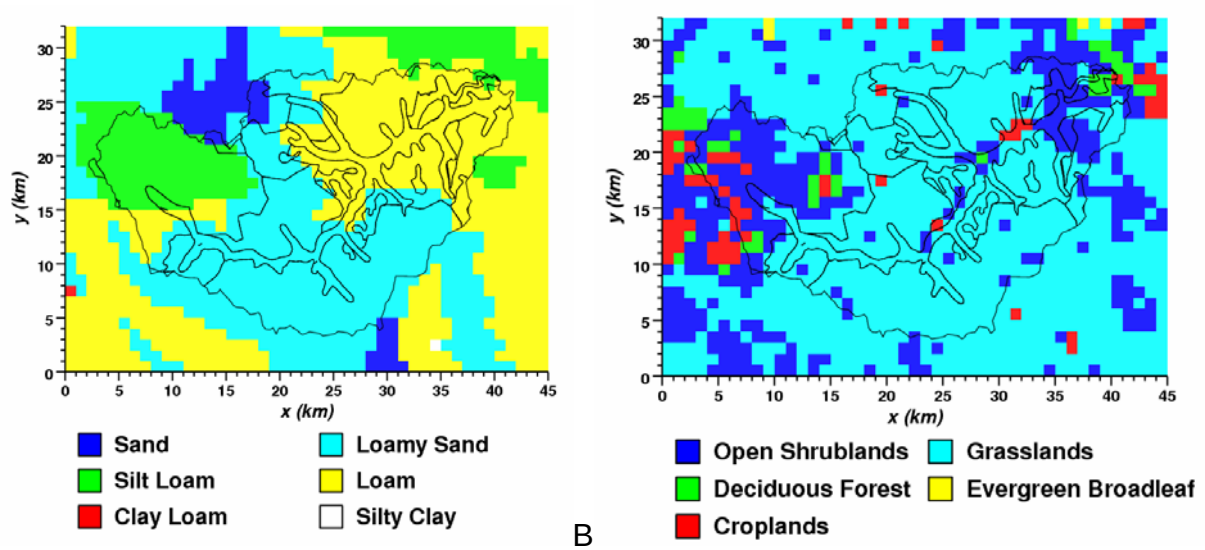

A B

Figure 3. Plot of a) soil type and b) vegetation type for the simulation.

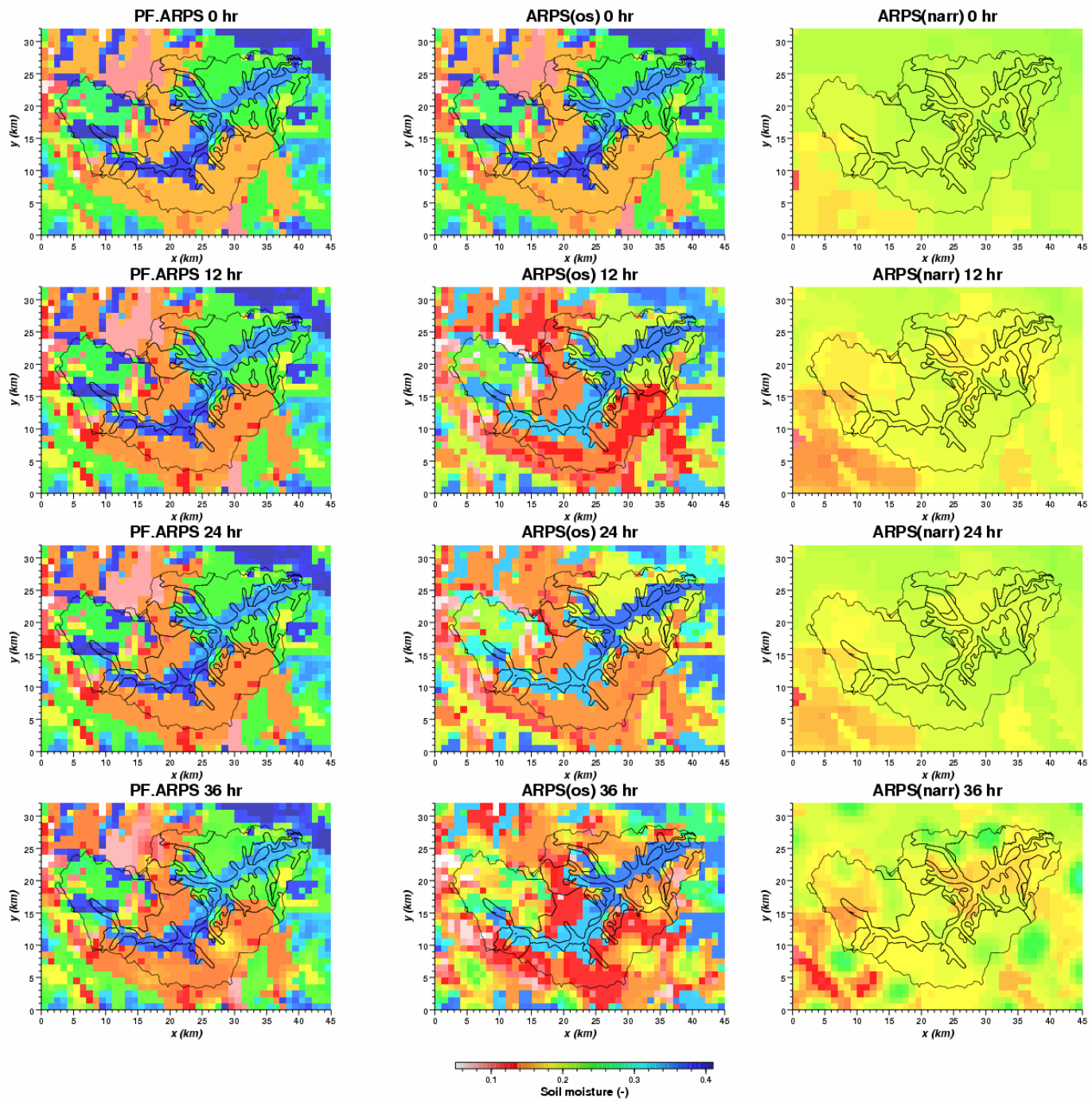

Figure 4. Plot of surface soil moisture for the PF.ARPS (left), ARPS(os) (middle) and ARPS(narr) (right) models at 12 h intervals from time zero to the end of the coupled simulation.

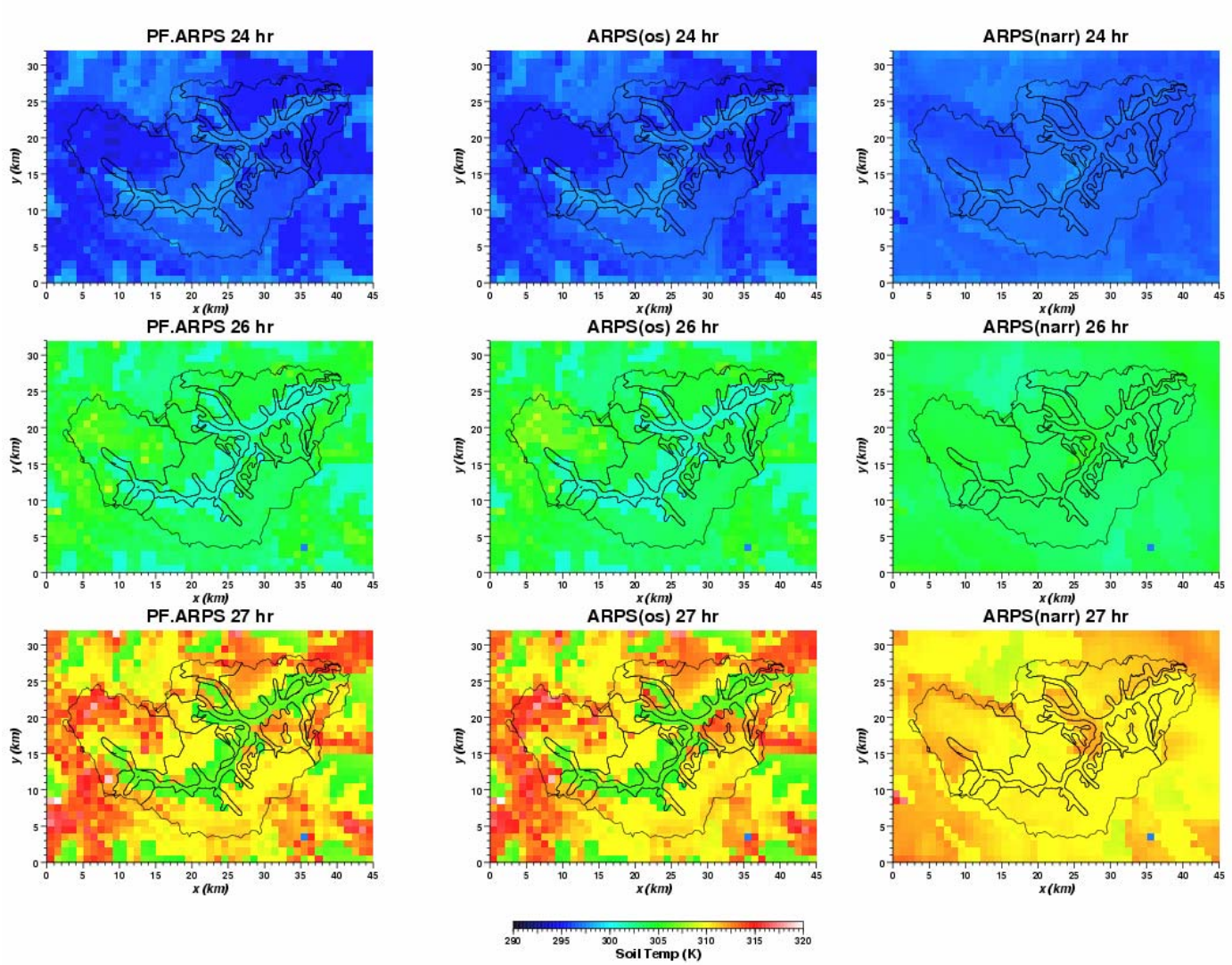

Figure 5. Plot of surface soil temperature for PF.ARPS (left), ARPS(os) (middle) and ARPS(narr) (right) at simulation times 24 (top), 26 (middle) and 27 (bottom) hours.

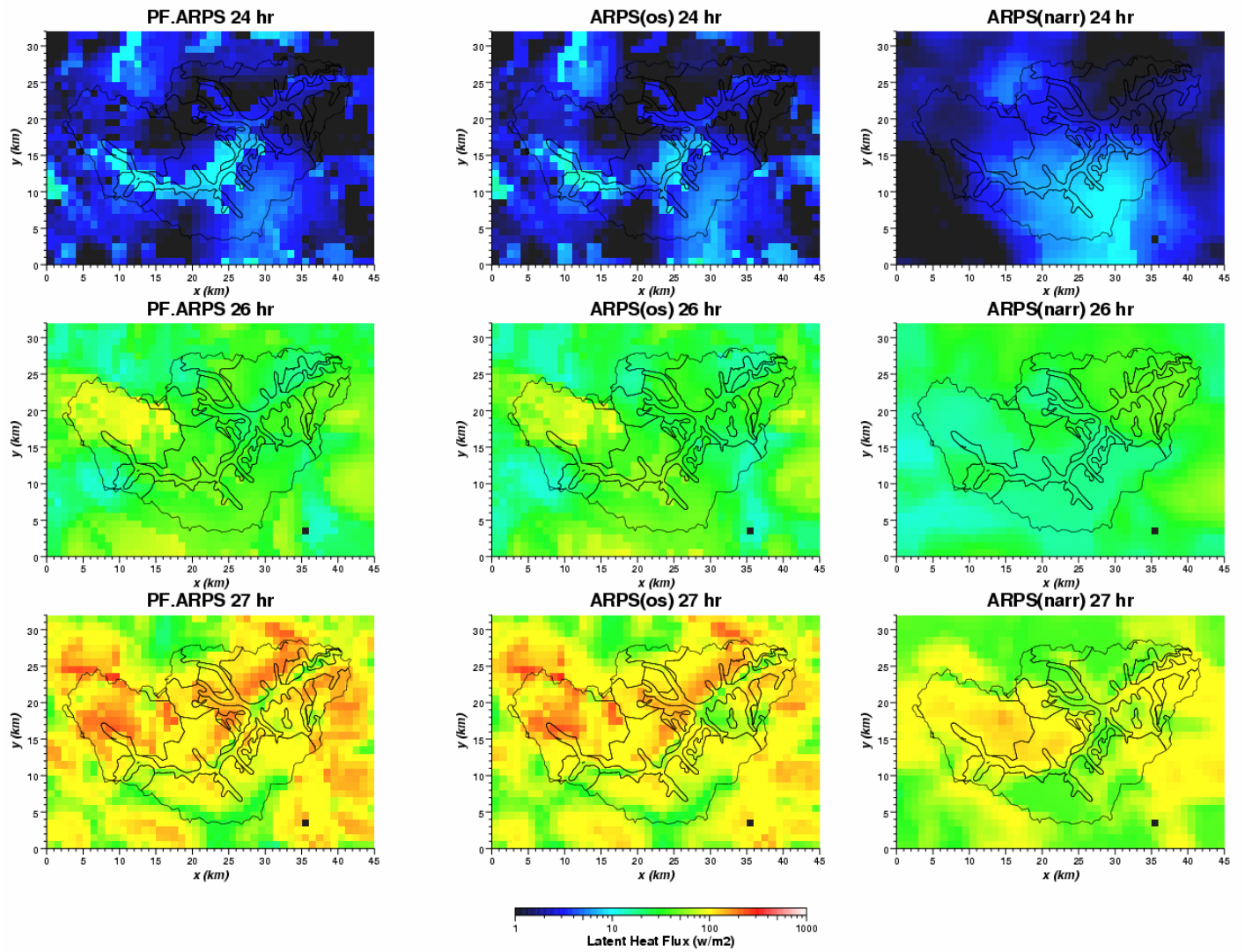

Figure 6. Plot of latent heat for PF.ARPS (left), ARPS(os) (middle) and ARPS(narr) (right) at simulation times 24 (top), 26 (middle) and 27 (bottom) hours. Note the log color scale for latent heat flux.

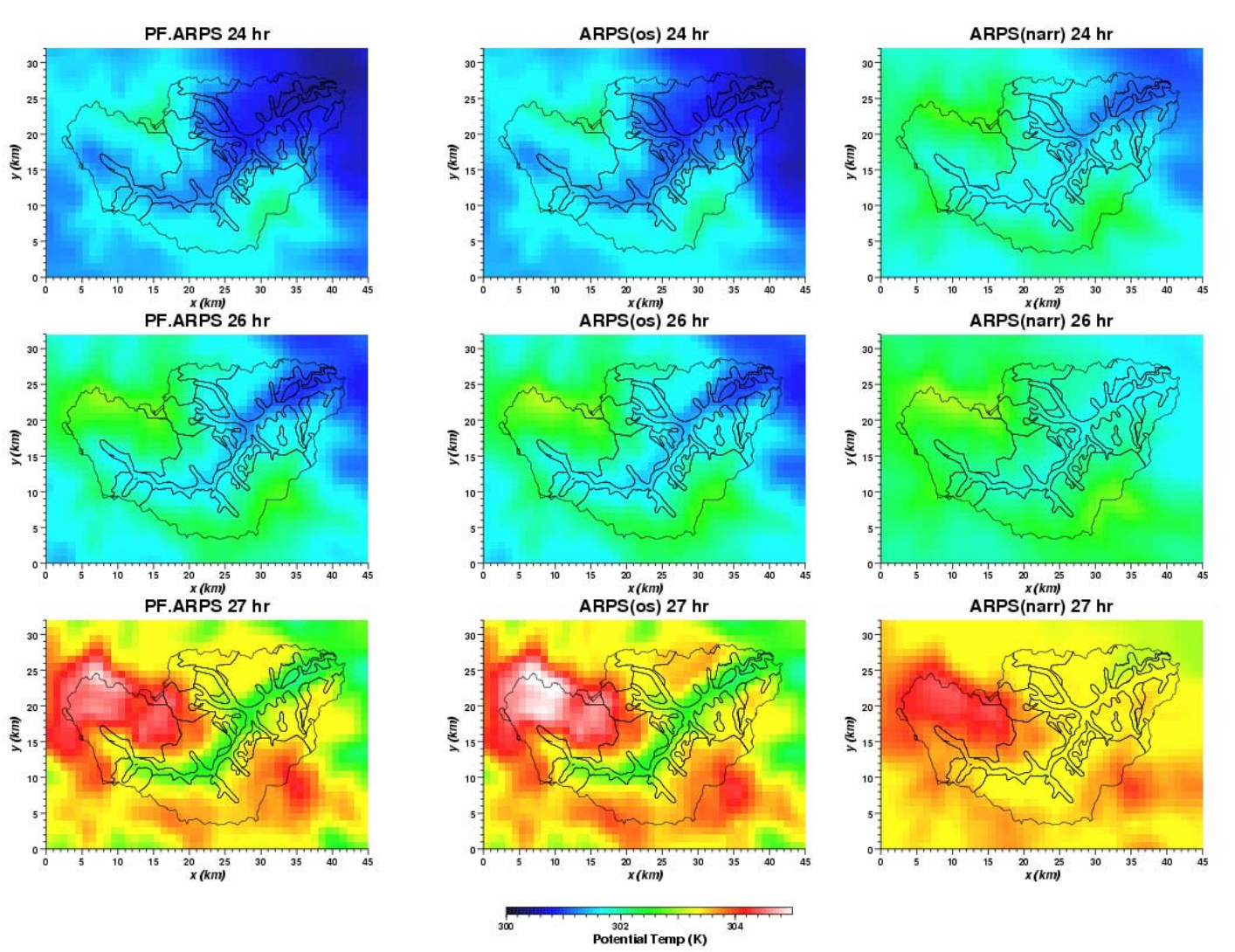

Figure 7. Plot of potential temperature for PF.ARPS (left), ARPS(os) (middle) and ARPS(narr) (right) at simulation times 24 (top), 26 (middle) and 27 (bottom) hours.

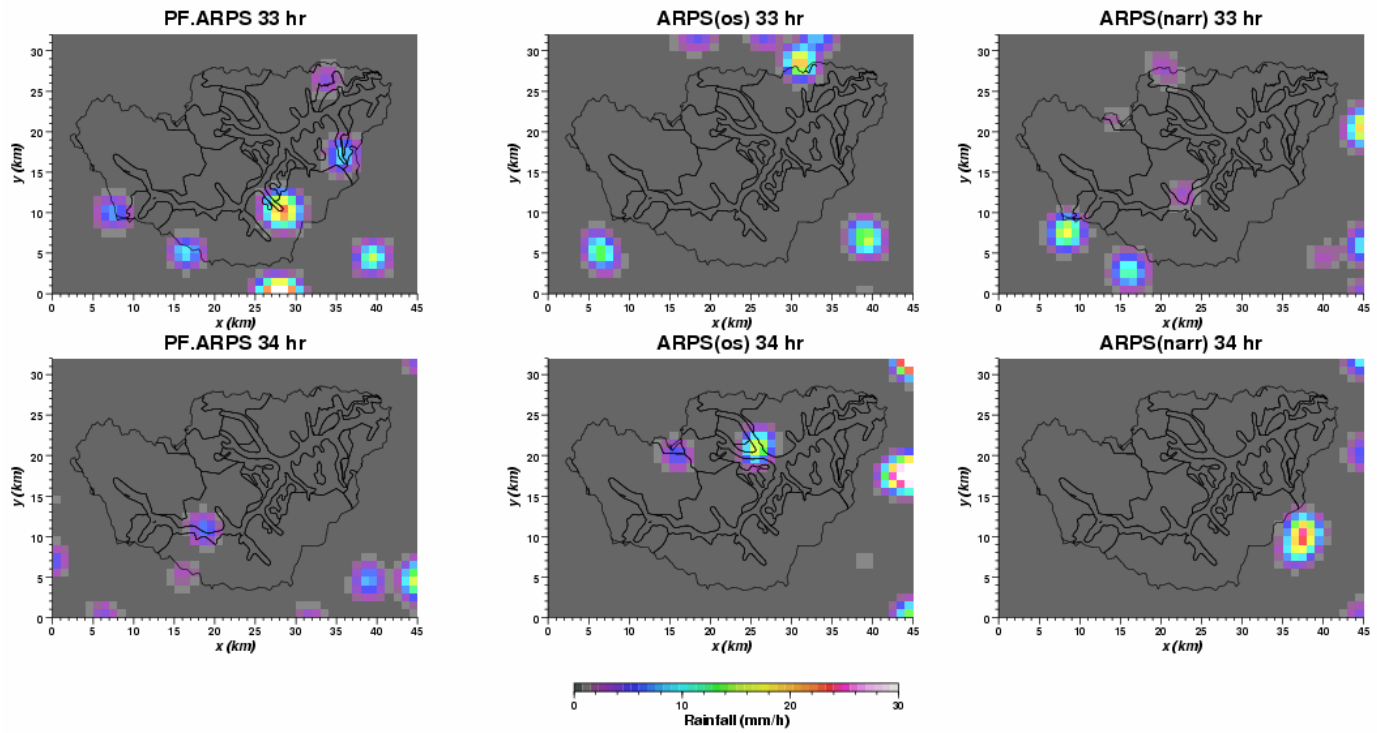

Figure 8. Plot of hourly rainfall for PF.ARPS (left), ARPS(os) (middle) and ARPS(narr) (right) at simulation times 33 (top) and 34 (bottom) hours.

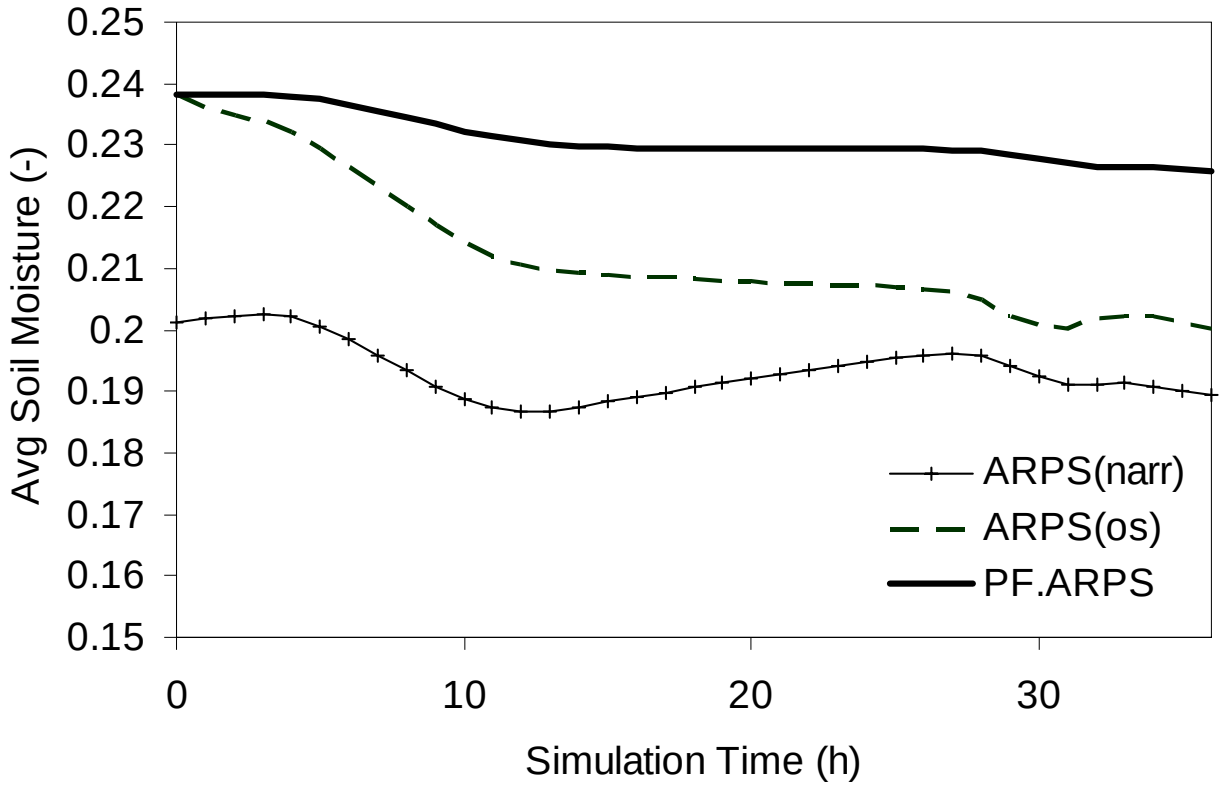

Figure 9. Plot of soil moisture (averaged over the domain) for the upper soil layer for the 36 hour simulation for three different test cases .

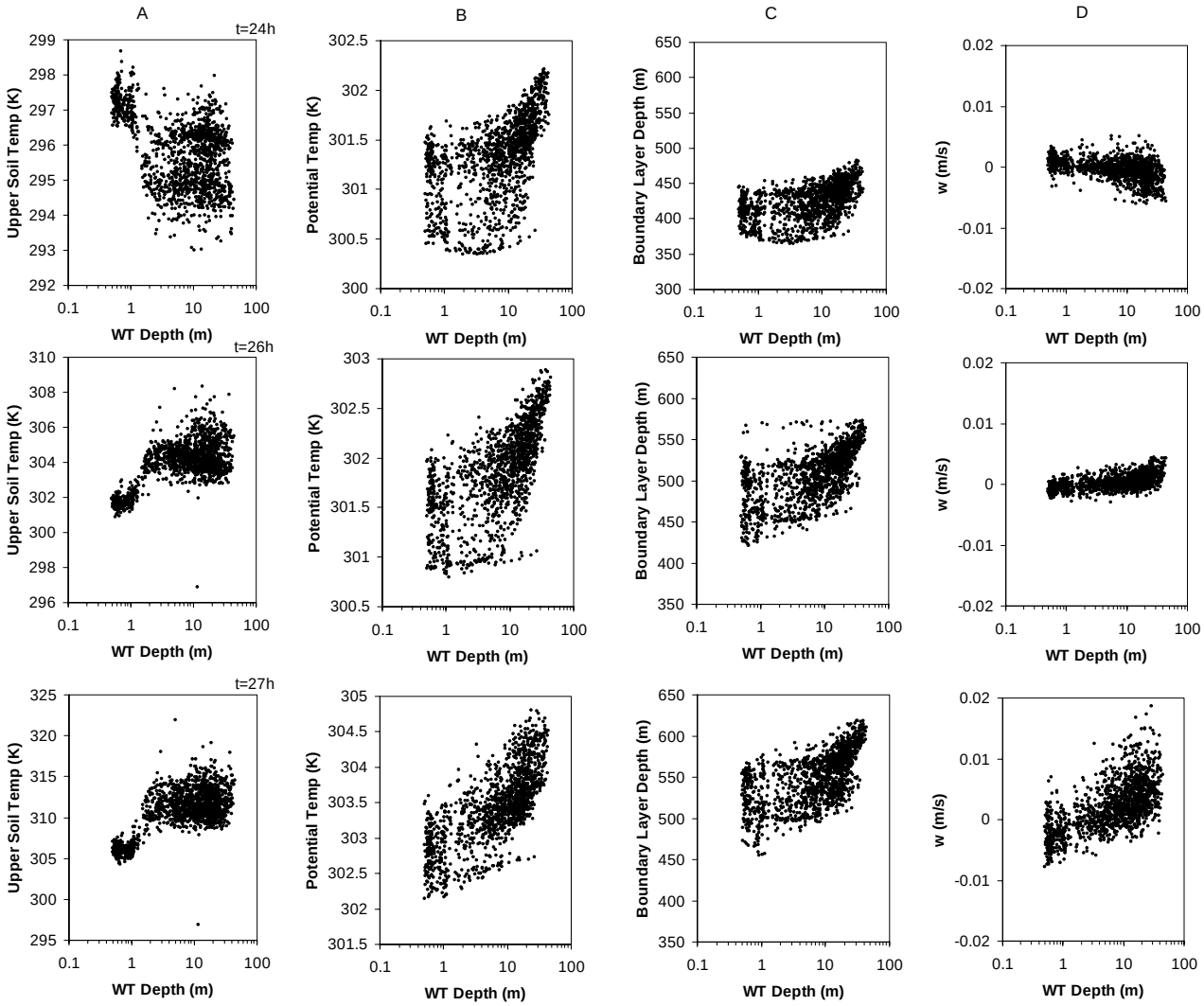

Figure 10. Semi logarithmic scatterplots of soil temperature (A), potential temperature (B), boundary layer depth (C) and vertical velocity (D) as a function of water table at simulation times 24 (top), 26 (middle) and 27 (bottom) hours. Note the different axis ranges in y for soil and potential temperature.

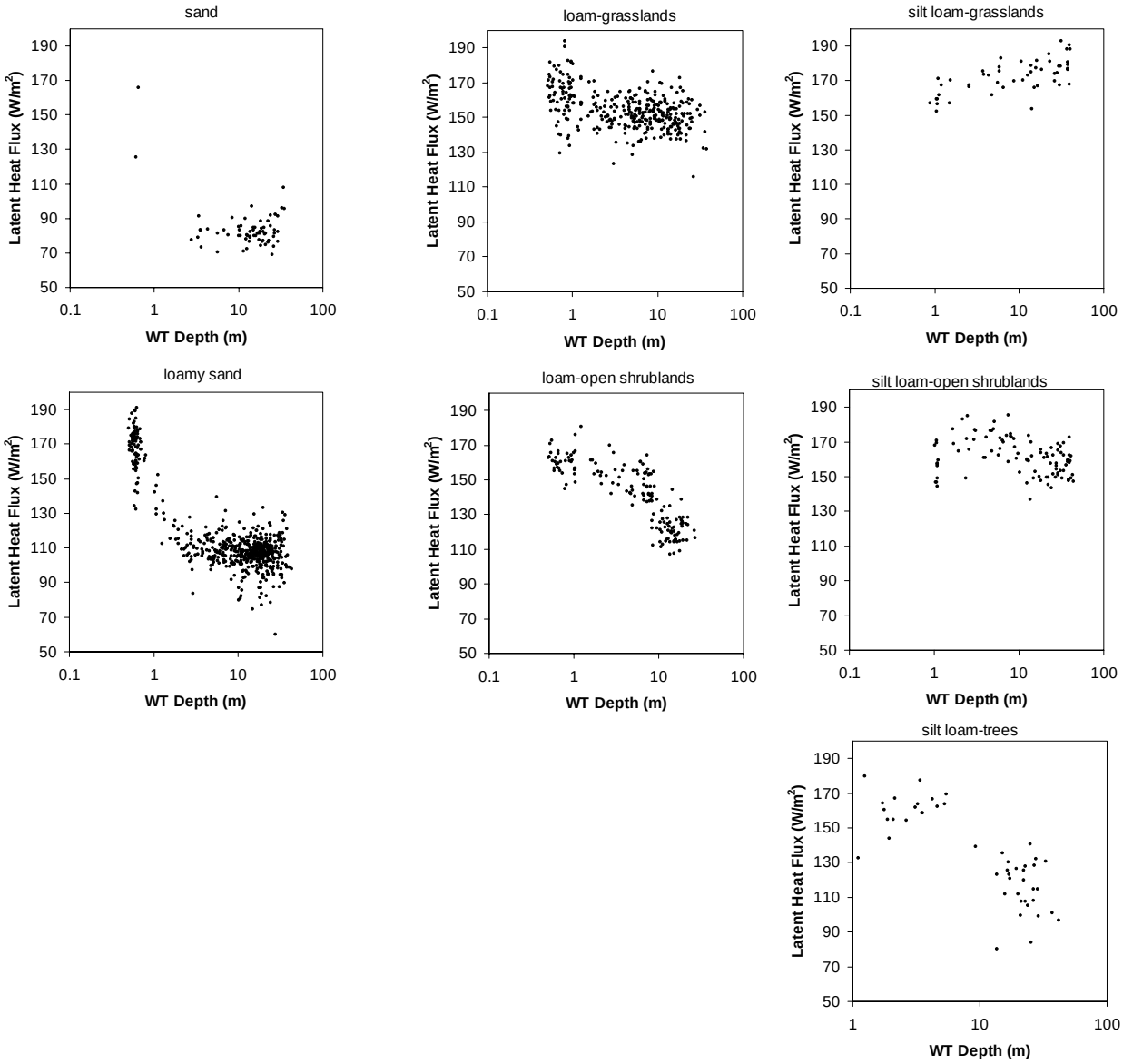

Figure 11. Semi logarithmic scatterplots of latent heat flux (averaged at each surface cell over the simulation time) as a function of water table (averaged over the simulation time) for a range of soil and vegetation types.

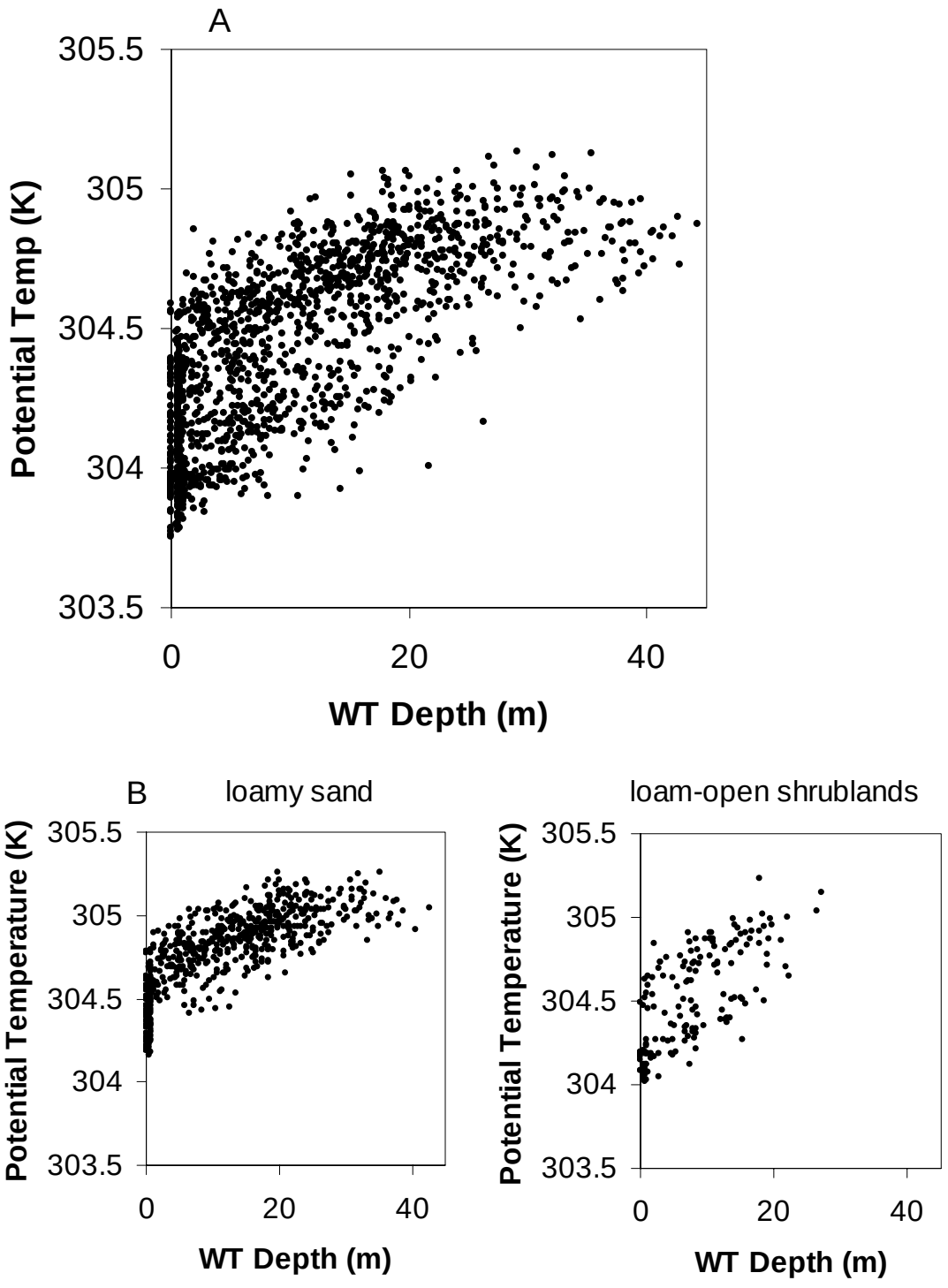

Figure 12a-b. Scatterplot of potential temperature (averaged at each lower atmospheric cell over the simulation time) as a function of water table (averaged over the simulation time), a) for all soil types and vegetation cover, b) for loamy sand (all vegetation types) and loam covered by open shrublands.